ACS APPLIED MATERIALS & INTERFACES

Research Article

www.acsami.org

Synthesis, Self-Assembly, and High Performance in Gas Sensing of X-Shaped Iron Oxide Crystals

Zhi-Feng Dou,[†,‡] Chang-Yan Cao,[†] Qiong Wang,[§] Jin Qu,[†] Yu Yu,[†] and Wei-Guo Song*[,†]

[†]Beijing National Laboratory for Molecular Sciences (BNLMS) & Key Laboratory of Molecular Nanostructure and Nanotechnology, Institute of Chemistry, Chinese Academy of Sciences, Beijing, 100190, P. R. China

[‡]Key Laboratory of Ministry of Education for Application Technology of Chemical Materials in Hainan Superior Resources, College of Materials and Chemical Engineering, Hainan University, Haikou, 570228, P. R. China

[§]State Key Laboratory of Applied Organic Chemistry, College of Chemistry and Chemical Engineering, Lanzhou University, Lanzhou, 730000, P. R. China

Supporting Information

ABSTRACT: X-shaped goethite iron oxide crystals were synthesized by a surfactant-free mild hydrothermal synthesis method with the aid of fluorine ions. The X-shaped goethite crystals could readily self-assemble into microscopic hollow spheres through an oil−water interface induced self-assembly method. X-shaped hematite crystals were obtained by phase topotactic transformation of the goethite precursors. The gas sensor properties of X-shaped hematite iron oxide were investigated, and the mechanism for excellent sensor properties was discussed.

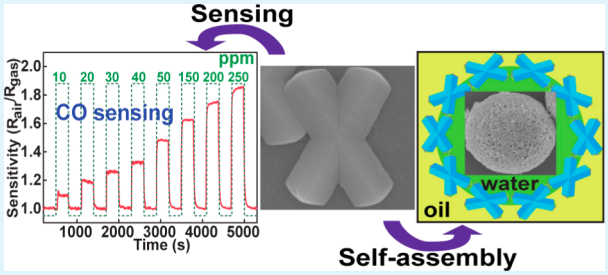

KEYWORDS: *hydrothermal synthesis, goethite, phase transformation, hematite, sensor, self-assembly*

1. INTRODUCTION

Over the past decades, synthesis and application of nanocrystals have attracted much attention due to their unique physical and chemical properties,[1−3] which are determined not only by their compositions and crystallographic structures but also by their size and morphology. Additionally, nanocrystals with anisotropic shapes, i.e., nonspherical shapes, are desirable for better control of the self-assembly process because anisotropic shapes help the nanocrystals to fit into the desired positions. In recent years, nanocrystals with nonspherical shapes including one-dimensional crystals (nanorod, nanotube, etc.), two-dimensional crystals (nanodisk, nanoprism, etc.), and three-dimensional crystals (nanomultipod, polyhedron, etc.) have been reported.[4−10]

Among a long list of nanocrystals, iron oxide nanocrystals have been one of the extensively investigated transition metal oxides. Their variable oxidation states and crystal structures, low cost, magnetic properties, and environmental friendly nature are appealing features for researchers. Accordingly, the synthesis of iron oxide nanocrystals with nonspherical shape has been one of the bright spots in material chemistry. For example, Yu et al. have synthesized monodisperse α-Fe_2O_3 nanorods with continuously tuned aspect ratio by a microwave-assisted hydrothermal method with the aid of a phosphate anion.[11] Yin et al. reported a synthesis method to produce low-symmetry iron oxide with high-index facets being exposed using sodium carboxymethyl cellulose as surfactant.[12] Yan et al. produced iron oxide nanorings by using a double anion-assisted hydrothermal method involving phosphate and sulfate ions.[13] However, it is still a tough task to fabricate iron oxide nanocrystals with anisotropy morphologies because the surface energies of their low-index planes are fairly similar, making it hard to exploit surface energy difference for shape control.[14,15]

In this study, we developed a simple method to obtain well-defined X-shaped hematite iron oxide (α-Fe_2O_3) crystals. This is a low cost and green method, using only sodium carbonate, sodium fluoride, iron chloride hexahydrate, and water as raw materials. Each branch of the X-shaped α-Fe_2O_3 was single crystals with high-index facets being exposed. These X-shaped iron oxide crystals showed excellent sensor properties for CO gas and hydrogen with a sensing limit as low as 10 ppm. Such X-shaped morphology also offers an anisotropic feature to further controllable self-assembly. By a simple ultrasonication-assisted interface-induced method, micrometer hollow spheres were produced from the self-assembly of these X-shaped crystals.

2. EXPERIMENTAL SECTION

2.1. Fabrication of X-Shaped α-Fe_2O_3. All the reagents used were AR grade and used as received. DI water was used throughout the experiment. The X-shaped goethite iron oxide nanocrystals were obtained through a simple hydrothermal process. Typically, 53 mg of sodium fluoride and 20 mg of sodium carbonate were added in an 80 mL aqueous solution of iron chloride hexahydrate (0.12 mM) under stirring for 15 min to form transparent solution. Then the mixed

Received: August 17, 2012
Accepted: September 26, 2012
Published: September 26, 2012

solution was transferred into a 100 mL Teflon-lined stainless steel autoclave, sealed, and kept at 150 °C for 12 h. The yellow products were collected by centrifugation at 5000 r/min and rinsed several times with deionized water before drying at 80 °C overnight. On the basis of the amount of dried yellow product, the yield of α-FeOOH was about 76%. The X-shaped α-Fe_2O_3 crystals were produced by heating as-prepared yellow products in air at 350−550 °C for 3h with a ramping rate of 2 °C/min.

2.2. Structure and Properties Characterization. The morphology and microstructures of products were examined by a field-emission scanning electron microscope (FESEM; JEOL, JSM-6700F, operated at 10 kV) and a high-resolution transmission electron microscope (HRTEM; JEOL, JEM-2100, 200 kV, with electron diffraction). The crystal structure and phase of the products were characterized with X-ray powder diffraction (XRD; Rigaku D/max-2500, filtered Cu K_α radiation λ = 0.1542 nm, at 40 kV and 100 mA). Raman spectra were collected on a Thermo Scientific Raman Microscope DXR with 532 nm laser excitation at room temperature and taken with a 50× microscope objective at 1 mW laser power on the sample. The nitrogen adsorption and desorption isotherms were measured on a Quantachrome Autosorb AS-1 instrument at 77 K with the samples degassed at 200 °C with 3 h under vacuum before measurements. Thermogravimetry analysis (TGA) was carried out on samples placed in corundum crucibles with a heating rate of 10 K/min (TA Q600 apparatus, USA). The gas-sensing experiments were performed on a homemade computer-controlled sensor system. The as-prepared α-Fe_2O_3 sensor materials were dropped on a UST sensor device after dispersing in water by ultrasonication. The sensing operating temperature was 300 °C for carbon monoxide and 250 °C for hydrogen, respectively, and the gas flow concentration was controlled using a digital mass flow controller.

2.3. Self-Assembly of X-Shaped Crystals. In a typical self-assembly experiment, 2.0 mg of yellow X-shaped goethite iron oxides was dispersed in 1.0 mL of water by ultrasonication to form yellow color stock solution. Then, 16 μL of stock solution was added in a vial filled with 2.0 mL of nitromethane under ultrasonication for 0.5 h. Again, formed faint yellow solution was put into the oven at 50 °C overnight under static conditions, after which a precipitate was obtained at the bottom of the vial. The precipitate was collected and transferred onto the conductive substrate for further analysis.

3. RESULTS AND DISCUSSION

3.1. Characteristics of X-Shaped Iron Oxide. X-shaped yellow goethite iron oxide (α-FeOOH) crystals were first produced by a mild hydrothermal synthesis method at 150 °C by using only sodium carbonate, sodium fluoride, iron chloride hexahydrate, and water as raw materials. No organic surfactant was used. XRD patterns (Figure 1a) confirmed that the initial yellow products after hydrothermal synthesis were pure orthorhombic phase goethite iron oxide (α-FeOOH, JCPDS 81-0462), and red products after heat treatment at 450 °C were rhombohedral phase hematite iron oxide (α-Fe_2O_3, JCPDS 33-0664).

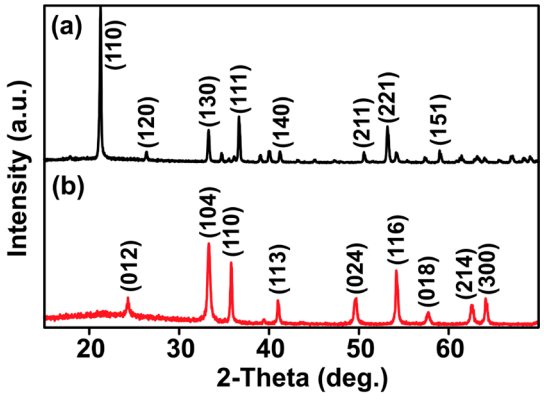

Figure 1. XRD patterns: (a) α-FeOOH produced from hydrothermal reactions and (b) α-Fe_2O_3 produced from topotactic transformation.

The morphology of the products was examined by SEM. Figure 2a shows representative SEM images of the α-FeOOH products after hydrothermal synthesis, indicating that the X-shaped α-FeOOH has uniform X-shaped morphology (Supporting Information, Figure S1a) composed of a quadrangular prism with rhombus cross sections (see inset in Figure 2a). As shown in Figure 2b, the morphology of the

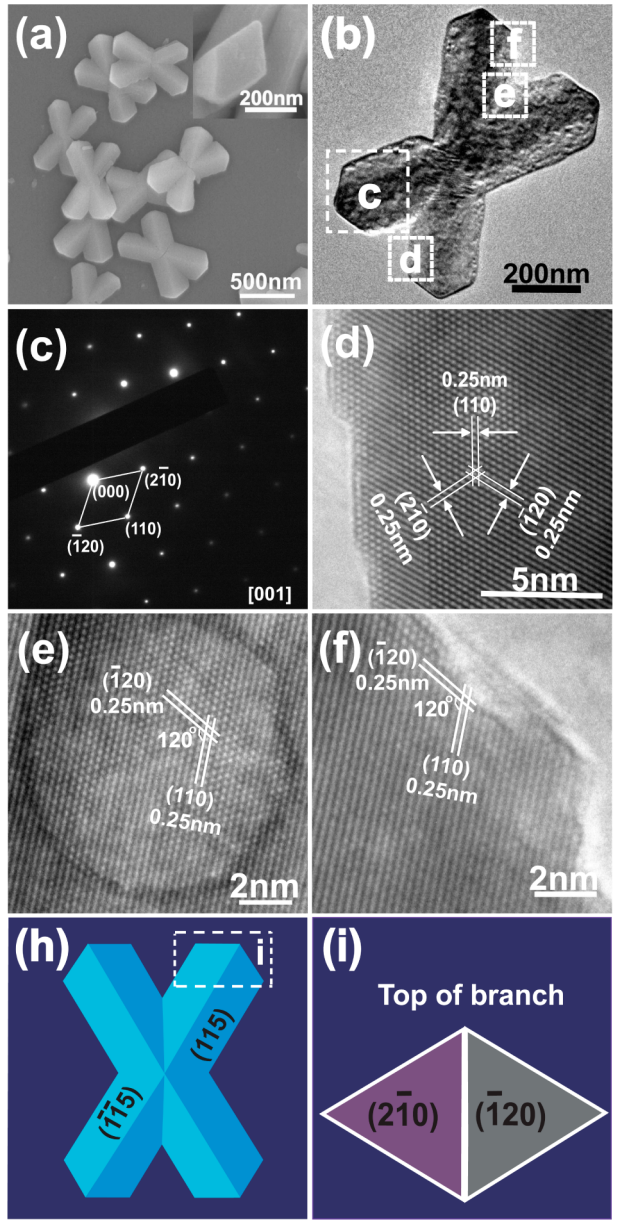

Figure 2. (a) SEM image of hydrothermal reaction products. Inset shows SEM image of an X-shaped crystal branch end. (b) TEM image of an X-shaped hematite iron oxide crystal heated at 450 °C for 3 h. (c) SAED pattern of X-shaped hematite iron oxide crystals projected from the [001] direction. (d, e, f) HRTEM images of an X-shaped hematite iron oxide crystal from positions labeled in (b, h, i). Structural model of the X-shaped hematite iron oxide crystals enclosed by high-index facets of {210} and {115}.

dx.doi.org/10.1021/am3016944 | ACS Appl. Mater. Interfaces 2012, 4, 5698−5703

hematite obtained by phase transformation remained as X-shaped. On the basis of high-resolution transmission electron microscope images (Figure 2d, 2e, and 2f) and SAED patterns (Figure 2c), each branch of the X-shaped α-Fe_2O_3 crystals was single crystal with the end facets of {210}. The side crystal planes of the X-shaped α-Fe_2O_3 crystals could be identified as {115} facets by calculation according to the crystallographic structure of hematite. Therefore, uniform X-shaped hematite crystals enclosed by high-index facets of {210} and {115} could be obtained by simple topotactic phase transformation as illustrated in Figure 2h and 2i.

3.2. Growth and Phase Transformation Mechanism of X-Shaped Iron Oxide. To investigate the growth mechanism of X-shaped goethite iron oxide crystals, time-dependent experiments were carried out. The hydrothermal reactions were conducted at 150 °C for 1−12 h, and SEM images of the products synthesized at different reaction times were shown in Figure 3. When the reaction time was as short as 1.0 h, the

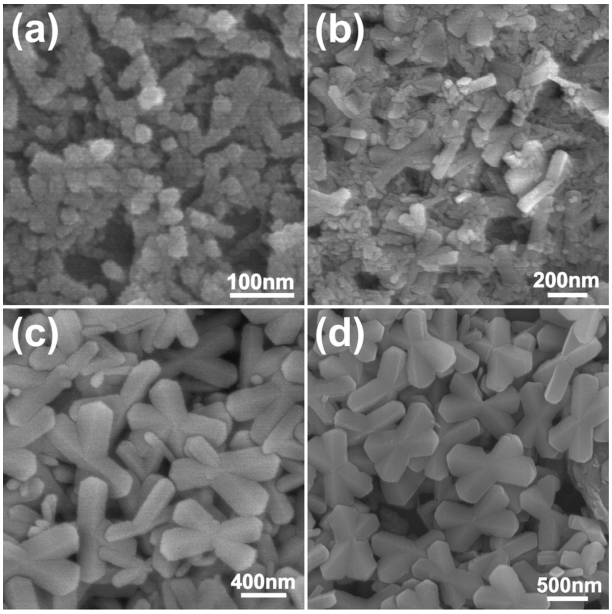

Figure 3. SEM images of the as-prepared products at 150 °C for different reaction times: (a) 1.0 h, (b) 2.0 h, (c) 4.0 h, and (d) 12 h.

product was irregular nanostructure with a diameter of about 30 nm (Figure 3a), and XRD patterns (Figure S2d, in the Supporting Information) indicated the products were akaganeite iron oxide (β-FeOOH). With the reaction continued further, small primary X-shaped goethite iron oxide (α-FeOOH) nanoparticles were formed (see Figure 3b and Figure S2c in the Supporting Information). As reaction time increased to 4 h, nearly all irregular nanoparticles had been transformed into X-shaped crystals, but there were small amounts of particles on the surfaces of X-shaped crystals. After 12 h, the morphology of the products was not changed, but their surfaces were free of small particles and were very smooth (Figure 3d). The size and morphology of the product remained the same at longer reaction time (e.g., 24 h).

It has become one of the most common strategies to change crystal plane surface energy by the introduction of inorganic ions, or small organic molecules in the reaction system, to control nanocrystal anisotropic growth.[16−18] In our present study, the fluoride anion was used to control the morphology of the X-shaped goethite precursor. Therefore, fluoride anion concentration-dependent experiments were conducted with other reagent concentrations, and experiment conditions remained the same. The results (Figure S3, in the Supporting Information) showed that only α-Fe_2O_3 single-crystal dodecahedral could be produced without a fluoride anion, and wheel-shaped polyhedra (α-FeOOH) were obtained at higher fluoride anion concentrations. X-shaped α-FeOOH could be produced only at suitable fluoride anion concentrations. This indicated that fluoride anion preferential adsorption at special facets might induce X-shaped products.

X-ray photoelectron spectroscopy (XPS), as an effective surface analysis method, was conducted to confirm the presence of fluoride. XPS results in Figure 4a showed that

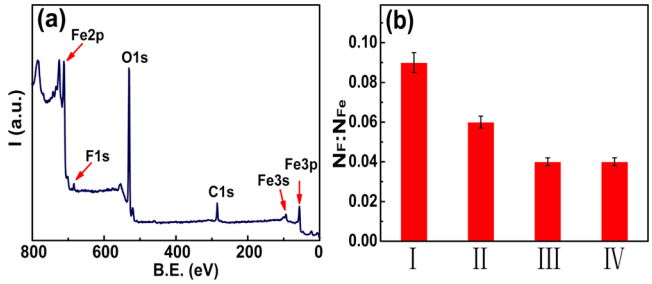

Figure 4. (a) Representative XPS spectra of X-shaped iron oxide. (b) Molar ratio of F to Fe at different sample surfaces: (I) unwashed X-shaped goethite products; (II) thoroughly washed X-shaped goethite products; (III) X-shaped hematite obtained by heating unwashed X-shaped goethite; (IV) X-shaped hematite obtained by heating thoroughly washed X-shaped goethite.

there was a small peak with binding energy at 685.2 eV, which originated from the F1s binding energy peak of Fe−F bonds.[19] However, no sodium element peaks were observed, confirming that the fluoride signal was from the fluoride attaching to the iron oxide surface, not from residual NaF. At the same time, XPS tests of different samples (see Figure S4, in the Supporting Information) treated under different conditions were carried out. Surface molar ratios of F to Fe were calculated based on the F1s and Fe2p peak areas of XPS spectra (see Figure 4b). The molar ratios of F to Fe decreased from the unwashed sample to the thoroughly washed sample, indicating that the some of the fluoride anions on the surface of the sample were not tightly bound. However, the amount of fluoride was constant after heating at 450 °C, indicating that these remaining fluoride species were tightly bonded to the iron oxide surface.

The above experimental results suggested that the growth of X-shaped goethite nanostructures underwent an oriented aggregation and recrystallization growth process, and the bonding of fluoride anions on certain surfaces played a key role in the morphology control. In the initial nucleation stage, ferric ions first hydrolyzed into disordered akaganeite (β-FeOOH) nanoparticles.[20] Subsequently, disordered akaganeite nanoparticles were gradually transformed into goethite, because goethite was a more stable thermodynamic phase, and started to form rods by oriented aggregation.[21] Anisotropy growth of primary goethite nanoparticles was possible with the aid of fluorine anions by a recrystallization growth process. During this process, fluoride anion preferential adsorption occurred on (010) faces of goethite and inhibited the growth rate at the [010] direction, resulting in twinned crystal growth at the [210]

dx.doi.org/10.1021/am3016944 | ACS Appl. Mater. Interfaces 2012, 4, 5698−5703

direction.[22] There are four equivalent ⟨210⟩ directions. With relative low fluoride anion concentrations, X-shaped goethite product could be obtained by twinned crystal growth along [210] and [-2-10] or [-210] and [2-10], respectively.

Goethite can be easily transformed into hematite at temperatures higher than 250 °C by phase topotactic transformation. The microstructure of the transformation products obtained by the dehydration process at different temperatures may be different, which may affect physical and chemical properties of the products.[23,24] It is believed that the dehydration of goethite was a three-dimensional diffusion process for water molecules.[25] TG analysis (Figure S5, in the Supporting Information) showed that there are three main weight loss stages: before 250 °C, between 250 and 300 °C, and above 300 °C. The weight loss before 250 °C was mainly ascribed to the loss of physical adsorbed water, and the weight loss in the range of 250 and 300 °C was due to the surface layer dehydration process, especially at places where surface area per unit volume was large (such as edges and surface steps). The weight loss above 300 °C was due to the dehydration reaction in bulky crystals and was relatively slow because the hematite layer formed at the surface layer hindered the diffusion of water molecules. The as-prepared X-shaped α-FeOOH crystals were heated at 350, 400, 450, 500, and 550 °C, respectively, to find the optimal temperature. As XRD patterns show in Figure S6 in the Supporting Information, all five samples were pure hematite (α-Fe_2O_3).

3.3. Sensor Property of X-Shaped Hematite. Hematite (α-Fe_2O_3), as one of the most important iron oxides with n-type semiconducting properties (E_g = 1.9−2.3 eV), is a very suitable sensor material owing to its nontoxicity, low cost, and high stability under ambient conditions.[10,16,26−30] The sensing performance of the as-prepared X-shaped α-Fe_2O_3 crystals for CO and H_2 was investigated. First, five X-shaped hematite samples produced at different temperature were tested for their properties as sensing materials for CO gas. Sensing data shown in Figure 5 suggested that topotactic transformation temperature had a profound influence on the sensing performance of α-Fe_2O_3 crystals. The sensitivity (defined as the ratio of the stationary electrical resistance of the sensor in air (R_{air}) to its resistance in the test gas (R_{gas})) increased as transformation temperature rose before reaching a maximum at 450 °C and then notably decreased as the temperature increased further. The samples prepared at 500 and 550 °C showed nearly the same sensitivities. As showed in Figure 5a, the sensitivity of all five X-shaped hematite crystals was much higher than commercial hematite powders.

The sensor properties of S450 (the X-shaped α-Fe_2O_3 crystals obtained at 450 °C) were investigated in detail. As shown in Figure 6a, the S450 sample showed fast and strong responses to CO gas with concentrations ranging from 10 to 250 ppm at 300 °C optimum operating temperature of sensors. The stability of X-shaped α-Fe_2O_3 crystals was tested under two different CO concentrations. Figure 6b shows that α-Fe_2O_3 crystals obtained at 450 °C exhibited outstanding sensor stability for CO gas at 300 °C optimum operating temperature of sensors. In 10 testing cycles, the response curves of each cycle were about the same, showing nearly no signal change or baseline drifting. The response and recovery times (defined as the time required to reach 90% of the equilibrium value) of the as-prepared α-Fe_2O_3-based sensors were 10.3 and 26.1 s for 50 ppm CO and 19.7 and 34.6 s for 200 ppm CO, respectively, indicating their excellent response and reversibility (Figure 6c).

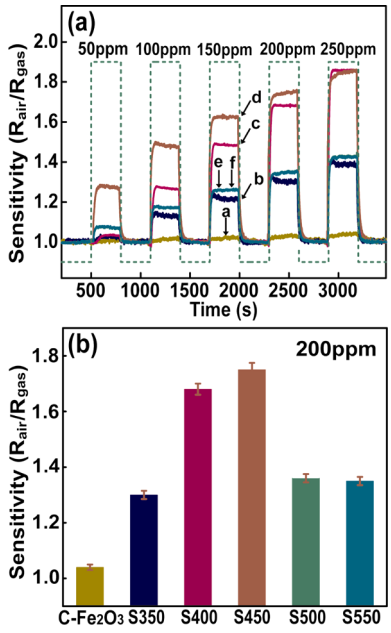

Figure 5. (a) Real-time CO gas sensing characterization based on commercially available and as-prepared α-Fe_2O_3 crystals at different phase transformation temperature. (b) Gas response versus different samples at 200 ppm CO concentration.

In addition, the X-shaped hematite crystals also showed excellent sensitivity and stability against hydrogen gas with concentrations ranging from 10 to 50 ppm (Figure S7 in the Supporting Information) at 250 °C optimum operating temperature of sensors.

The specific surface area of X-shaped hematite crystals estimated from the BET method was 7.6 m^2/g (Figure S8, in the Supporting Information), which was relatively low compared with other iron oxide nanomaterials.[27,29] Therefore, the superior gas-sensing performance of X-shaped hematite crystals is more likely due to the nature of their special surface structure and crystallography structure.

The Raman spectra (Figure S9, in the Supporting Information) of X-shaped hematite (α-Fe_2O_3) crystals obtained from different topotactic transformation temperature showed noticeable differences, though their XRD patterns were identical. With the increase of transformation temperature, typical phonon lines of hematite at 218, 238, 285, 399, 489, 604, and 654 cm^{-1} became sharper. At 450 °C, the 654 cm^{-1} peak attributed to surface defects and local lattice disorder at the interfaces and interior faces reached a maximum.[31] Abundant unsaturated edges, atomic steps, and crystal defects were present at the surface of α-Fe_2O_3, which could act as active sites to adsorb target gases. At the same time, XRD and Raman data indicated that X-shaped hematite crystals obtained at 450 °C were well crystallized, which was favorable to improve electron conductivity and was beneficial to metal oxide gas sensors.[32,33] In addition, each crystal was enclosed by high-index planes, which was very favorable to improve the sensor performance.[16]

3.4. Self-Assembly of X-Shaped Goethite. Self-assembly of nanoscale building blocks has been a fascinating topic in material chemistry. Compared with isotropic spherical building blocks, which tend to form densely packed structures, building units with anisotropic shapes are better suited for programmed assembly into desired complex structures through anisotropic

dx.doi.org/10.1021/am3016944 | ACS Appl. Mater. Interfaces 2012, 4, 5698−5703

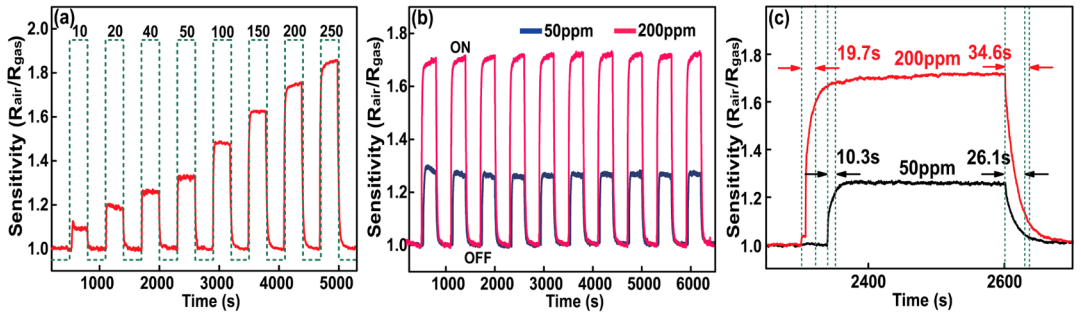

Figure 6. (a) Sensitivity toward different CO gas concentrations, unit ppm. (b) Stability at 50 and 200 ppm CO gas concentration. (c) Response and recovery times of the as-prepared α-Fe_2O_3 at 50 and 200 ppm CO concentration.

assembly.[5] New methods have been reported to induce the assembly of various nanocrystals.[34−37] The X-shaped crystals developed in this study have a unique shape. Their four corners as well as the cross junction in the middle are ideal contact positions for anisotropic assembly. As a preliminary trial, an oil−water interface induced self-assembly method was used to promote the self-assembly of X-shaped goethite crystals. In this study, microscale hollow spheres were obtained by this method. As shown in Figure 7a, the diameter of the hollow sphere

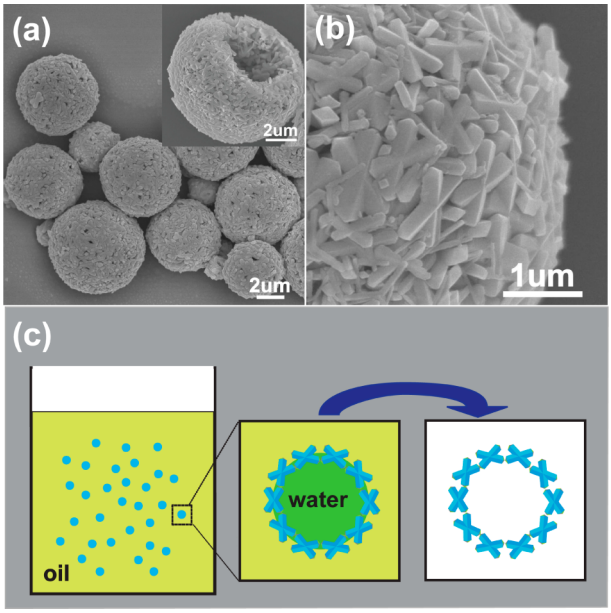

Figure 7. (a) SEM image of a micrometer scale hollow sphere from the self-assembly of the X-shaped goethite crystals. Inset shows a broken hollow sphere showing the hollow interior. (b) Enlarged SEM self-assembly of X-shaped goethite crystals. (c) Schematic representation of the self-assembly of X-shaped nanoparticles at the oil−water interface.

ranged from 3 to 10 μm. An enlarged SEM image (Figure 7b) of the spheres showed that the X-shaped building blocks tangled with each other by interdigitizing of the branches to form densely packed walls of the hollow spheres. When the assembled hollow spheres were heated at 450 °C for 3 h in air, the hollow sphere structure was preserved (see Figure S1b, in the Supporting Information), indicating the good thermal stability of the hollow spheres.

The self-assembly of nanocrystals at the oil−water interface depended on the balance among particle−particle interactions, particle−water interactions, and particle−oil interactions.[38,39] Such self-assembly of the X-shaped goethite crystals into a micrometer hollow sphere was mainly driven by the decrease of the total free energy at the oil−water interface. As depicted in Figure 7c, when the aqueous suspension of X-shaped goethite crystals was mixed with nitromethane by vigorous ultrasonication, water in oil micelles were produced. X-shaped goethite crystals would be prone to stack at the water−oil interface to decrease the total free energy of the system because interface energy between goethite and nitromethane was lower than that between water and nitromethane. A hollow sphere structure was then formed when the X-shaped goethite crystals were assembled at the oil−water interface of each micelle. After slow evaporation of water and nitromethane, assembled micrometer-scale hollow spheres composed of X-shaped goethite crystals were produced

4. CONCLUSIONS

In summary, X-shaped goethite (α-FeOOH) crystals were synthesized by a mild hydrothermal synthesis method with the aid of a fluoride anion and without any surfactant. Subsequently, hematite (α-Fe_2O_3) crystals with the same morphology were obtained by phase topotactic transformation. The X-shaped hematite crystals prepared under optimal conditions showed excellent sensor performance for CO and H_2 gases. Self-assembled microscopic hollow spheres were produced from oil−water interface induced self-assembly, as the anisotropic X-shaped goethite crystals acted as building blocks.

■ ASSOCIATED CONTENT

Supporting Information

SEM images of large-scale X-shaped goethite and products synthesized at different fluorine ion concentration, XRD patterns, micro-Raman spectra, XPS spectra of different samples, TGA curve, nitrogen adsorption−desorption isotherm, and sensor test results for hydrogen. This material is available free of charge via the Internet at http://pubs.acs.org.

■ AUTHOR INFORMATION

Corresponding Author

*E-mail: wsong@iccas.ac.cn. Fax: +86 10-62557908. Tel.: +86 10-62557908.

Notes

The authors declare no competing financial interest.

■ ACKNOWLEDGMENTS

We thank the financial support from the National Basic Research Program of China (2009CB930400), National

Natural Science Foundation of China (NSFC21121063), and the Chinese Academy of Sciences.

REFERENCES

(1) Zhou, Z.-Y.; Tian, N.; Li, J.-T.; Broadwell, I.; Sun, S.-G. *Chem. Soc. Rev.* **2011**, *40*, 4167−4185.
(2) Xia, Y.; Xiong, Y.; Lim, B.; Skrabalak, S. E. *Angew. Chem., Int. Ed.* **2009**, *48*, 60−103.
(3) Sau, T. K.; Rogach, A. L.; Jäckel, F.; Klar, T. A.; Feldmann, J. *Adv. Mater.* **2010**, *22*, 1805−1825.
(4) Yan, W.; Fan, H.; Yang, C. *Mater. Lett.* **2011**, *65*, 1595−1597.
(5) Glotzer, S. C.; Solomon, M. J. *Nat. Mater.* **2007**, *6*, 557−562.
(6) Tang, Z.; Zhang, Z.; Wang, Y.; Glotzer, S. C.; Kotov, N. A. *Science* **2006**, *314*, 274−278.
(7) Deka, S.; Miszta, K.; Dorfs, D.; Genovese, A.; Bertoni, G.; Manna, L. *Nano Lett.* **2010**, *10*, 3770−3776.
(8) Leng, M.; Liu, M.; Zhang, Y.; Wang, Z.; Yu, C.; Yang, X.; Zhang, H.; Wang, C. *J. Am. Chem. Soc.* **2010**, *132*, 17084−17087.
(9) Henzie, J.; Grünwald, M.; Widmer-Cooper, A.; Geissler, P. L.; Yang, P. *Nat. Mater.* **2012**, *11*, 131−137.
(10) Huang, L.; Fan, H. *Sens. Actuators, B* **2012**, *171−172*, 1257−1263.
(11) Hu, X.; Yu, J. C. *Adv. Funct. Mater.* **2008**, *18*, 880−887.
(12) Yin, J.; Yu, Z.; Gao, F.; Wang, J.; Pang, H.; Lu, Q. *Angew. Chem., Int. Ed.* **2010**, *49*, 6328−6332.
(13) Jia, C.-J.; Sun, L.-D.; Luo, F.; Han, X.-D.; Heyderman, L. J.; Yan, Z.-G.; Yan, C.-H.; Zheng, K.; Zhang, Z.; Takano, M.; Hayashi, N.; Eltschka, M.; KlaÜi, M.; RÜdiger, U.; Kasama, T.; Cervera-Gontard, L.; Dunin-Borkowski, R. E.; Tzvetkov, G.; Raabe, J. R. *J. Am. Chem. Soc.* **2008**, *130*, 16968−16977.
(14) Lv, B.; Liu, Z.; Tian, H.; Xu, Y.; Wu, D.; Sun, Y. *Adv. Funct. Mater.* **2010**, *20*, 3987−3996.
(15) Van, T.-K.; Cha, H. G.; Nguyen, C. K.; Kim, S.-W.; Jung, M.-H.; Kang, Y. S. *Cryst. Growth Des.* **2012**, *12*, 862−868.
(16) Yang, Y.; Ma, H.; Zhuang, J.; Wang, X. *Inorg. Chem.* **2011**, *50*, 10143−10151.
(17) Wang, X.; Chen, X.; Gao, L.; Zheng, H.; Ji, M.; Tang, C.; Shen, T.; Zhang, Z. *J. Mater. Chem.* **2004**, *14*, 905−907.
(18) Cao, M.; Liu, T.; Gao, S.; Sun, G.; Wu, X.; Hu, C.; Wang, Z. L. *Angew. Chem., Int. Ed.* **2005**, *44*, 4197−4201.
(19) Grosvenor, A. P.; Kobe, B. A.; Biesinger, M. C.; McIntyre, N. S. *Surf. Interface Anal.* **2004**, *36*, 1564−1574.
(20) Mackay, A. L. *Mineral. Mag.* **1962**, *33*, 270−280.
(21) Cudennec, Y.; Lecerf, A. *J. Solid State Chem.* **2006**, *179*, 716−722.
(22) Cornell, R. M.; Schwertmann, U. *The Iron Oxides: Structure, Properties, Reactions, Occurrence and Uses*; VCH: Weinheim, 2003; p 71.
(23) Gualtieri, A. F.; Venturelli, P. *Am. Mineral.* **1999**, *84*, 895−904.
(24) Cudennec, Y.; Lecerf, A. *Solid State Sci.* **2005**, *7*, 520−529.
(25) Fan, H.; Song, B.; Li, Q. *Mater. Chem. Phys.* **2006**, *98*, 148−153.
(26) Chen, J.; Xu, L.; Li, W.; Gou, X. *Adv. Mater.* **2005**, *17*, 582−586.
(27) Wu, Z.; Yu, K.; Zhang, S.; Xie, Y. *J. Phys. Chem. C* **2008**, *112*, 11307−11313.
(28) Zhang, F.; Yang, H.; Xie, X.; Li, L.; Zhang, L.; Yu, J.; Zhao, H.; Liu, B. *Sens. Actuators, B* **2009**, *141*, 381−389.
(29) Sun, B.; Horvat, J.; Kim, H. S.; Kim, W.-S.; Ahn, J.; Wang, G. *J. Phys. Chem. C* **2010**, *114*, 18753−18761.
(30) Yan, W.; Fan, H.; Zhai, Y.; Yang, C.; Ren, P.; Huang, L. *Sens. Actuators, B* **2011**, *160*, 1372−1379.
(31) Bersani, D.; Lottici, P. P.; Montenero, A. *J. Raman Spectrosc.* **1999**, *30*, 355−360.
(32) Wang, C.; Yin, L.; Zhang, L.; Xiang, D.; Gao, R. *Sensors* **2010**, *10*, 2088−2106.
(33) Comini, E.; Baratto, C.; Faglia, G.; Ferroni, M.; Vomiero, A.; Sberveglieri, G. *Prog. Mater. Sci.* **2009**, *54*, 1−67.
(34) Disch, S.; Wetterskog, E.; Hermann, R. l. P.; Salazar-Alvarez, G.; Busch, P.; BrÜckel, T.; Bergström, L.; Kamali, S. *Nano Lett.* **2011**, *11*, 1651−1656.
(35) Huang, T.; Zhao, Q.; Xiao, J.; Qi, L. *ACS Nano* **2010**, *4*, 4707−4716.
(36) Goodman, M. D.; Zhao, L.; DeRocher, K. A.; Wang, J.; Mallapragada, S. K.; Lin, Z. *ACS Nano* **2010**, *4*, 2043−2050.
(37) Miszta, K.; de Graaf, J.; Bertoni, G.; Dorfs, D.; Brescia, R.; Marras, S.; Ceseracciu, L.; Cingolani, R.; van Roij, R.; Dijkstra, M.; Manna, L. *Nat. Mater.* **2011**, *10*, 872−876.
(38) Xia, Y.; Nguyen, T. D.; Yang, M.; Lee, B.; Santos, A.; Podsiadlo, P.; Tang, Z.; Glotzer, S. C.; Kotov, N. A. *Nat. Nanotechnol.* **2011**, *6*, 580−587.
(39) Boker, A.; He, J.; Emrick, T.; Russell, T. P. *Soft Matter* **2007**, *3*, 1231−1248.